Available online at www.CivileJournal.org

Civil Engineering Journal

(E-ISSN: 2476-3055; ISSN: 2676-6957)

Vol. 12, No. 05, May, 2026

# Factors and Kinetics of Fat, Oil and Grease Deposit Formation in Kitchen Wastewater

Xin Yan [1], Dongyang Ren [1], Jingtao Feng [2], Zhi Tang [3], Zheng Fang [3*]

[1] School of Ecology and Environment, North China University of Water Resources and Electric Power, Zhengzhou 450046, China.

[2] Henan Province Construction Group Company Limited, Zhengzhou 450000, China.

[3] School of Civil Engineering, Wuhan University, Wuhan 430072, China.

Received 07 January 2026; Revised 23 April 2026; Accepted 27 April 2026; Published 01 May 2026

**Abstract**

This study systematically investigated key parameters influencing fat, oil, and grease (FOG) deposit formation in kitchen wastewater and elucidated the underlying chemical kinetics. Gas chromatography–mass spectrometry (GC–MS) was employed to characterize the composition of FOG deposits. Single-factor experiments and response surface methodology were used to identify the most significant factors contributing to saponification and determine optimal conditions for FOG accumulation. GC–MS demonstrated lower quantitative error rates than Fourier transform infrared (FTIR) spectroscopy and acid–base titration, with oleic acid identified as the predominant free fatty acid (FFA) component. The optimal saponification conditions were as follows: $C_{18}H_{34}O_2$:$CaCl_2$ mass ratio of 1:1.40, pH value of 7, reaction temperature of 30°C, and reaction duration of 1440 min, under which the maximum predicted saponification extent was 77.932%. Additionally, the kinetic model showed that FOG saponification followed a second-order reaction, with an activation energy of 53.1 kJ·mol$^{-1}$ and a pre-exponential factor of 5.4 × 10$^7$ L·mol$^{-1}$·min$^{-1}$. Overall, this research enhances the existing theoretical framework of FOG deposit formation by integrating engineering simulation with chemical kinetics and provides quantitative parameters to directly inform pipeline blockage mitigation and wastewater treatment optimization.

*Keywords:* Fat, Oil and Grease Deposits; Kitchen Wastewater; Chemical Formation; Influencing Factors; Kinetics.

## 1. Introduction

With the improvement of living standards, the consumption of meat, poultry, and dairy products in household and commercial catering settings has increased [1, 2]. As a result, considerable fat, oil, and grease (FOG) accumulation has been reported in the drainage pipes of household and restaurant kitchens, causing severe pipe blockage [3]. Fatty acid calcium salts are formed via saponification of free fatty acids (FFAs) in kitchen wastewater with $Ca^{2+}$ from food residues. These salts subsequently aggregate via physical deposition to form FOG deposits [4]. Thus, saponification plays a critical role in FOG deposit formation. The roles of FFAs, $Ca^{2+}$, and other factors in FOG deposit formation must be deeply investigated [5]. Such research will advance the theoretical understanding of FOG deposition and provide practical insights for preventing pipe blockages, optimizing wastewater treatment, and improving urban sanitation.

Increasing carbon chain length and the number of branches inhibits the hydrolysis of long-chain fatty acids during saponification [6]. FFAs such as palmitic acid ($C_{16}H_{32}O_2$) and oleic acid ($C_{18}H_{34}O_2$) are more prone to forming FOG deposits compared to lauric acid and linoleic acid [7]. Nevertheless, the relative susceptibility of different FFA species

* Corresponding author: zfang@whu.edu.cn

https://doi.org/10.28991/CEJ-2026-012-05-016

© 2026 by the authors. Licensee C.E.J, Tehran, Iran. This article is an open access article distributed under the terms and conditions of the Creative Commons Attribution (CC-BY) license (http://creativecommons.org/licenses/by/4.0/).

to saponification, and how this relates to deposit formation, have not been systematically analyzed. Using calcium chloride ($CaCl_2$) as the calcium source in simulated kitchen wastewater results in fatty acid salts with a white, loose structure, whereas calcium hydroxide ($Ca(OH)_2$) and calcium sulfate ($CaSO_4$) yield granular and coarse fatty acid salts. In line with these observations, Wu et al. [8] reported that FOG deposits formed in the presence of $Ca(OH)_2$ exhibited a higher degree of completion during saponification compared to those formed in the presence of $CaCl_2$ and $CaSO_4$. Subsequently, several studies have confirmed the key role of $Ca^{2+}$ in FOG deposition within practical engineering conditions. For example, Sultana et al. [9] reported that the use of $Ca(OH)_2$ and $Mg(OH)_2$ as biocorrosion control measures in municipal pipe networks increased FOG deposition. Further, Yusuf et al. [10] detected considerable concentrations of $Ca^{2+}$ in scum samples and effluents from multiple grease interceptors, which were considerably higher than those of $Fe^{2+}$, $Fe^{3+}$, $Mg^{2+}$, and $K^+$. However, calcium's contribution to saponification remains qualitative, lacking quantitative validation.

Environmental conditions such as temperature and pH also impact FOG deposition. Calcium remains as free $Ca^{2+}$ at low pH and combines with FFAs at neutral pH. In contrast, alkaline conditions trigger saponification to yield calcium fatty acid salts [11]. In addition, FOG deposits may melt in high-temperature water sewers, where they undergo saponification with calcium to generate large amounts of calcium fatty acid salts [12]. Iasmin et al. [13] reported that FOG deposits synthesized at 22°C and 45°C exhibited distinct infrared stretching vibration peaks and structural characteristics, further confirming the influence of temperature on FOG production. However, the effects of the FFA:$Ca^{2+}$ mass ratio and saponification time on FOG deposit formation have not been experimentally verified. Consequently, theoretical guidance for inhibiting FOG deposit formation and facilitating their removal from kitchen drainage systems is lacking.

The accurate determination of saponification extent is therefore a prerequisite for establishing such theoretical guidance. Currently, FTIR spectroscopy and acid–base titration are the primary methods employed for this purpose. FTIR analysis can be used to calculate the proportion of fatty acid calcium relative to total fat and grease based on vibrational modes [14, 15]. Iasmin et al. [16] modified the saponification rate equation based on infrared spectral quantification and determined the saponification extent by calculating the absorbance of characteristic soap bands from the FTIR spectrum. Kusum et al. [17] observed two strong asymmetric stretching vibrations at 1541 and 1577 $cm^{-1}$ corresponding to calcium soap and further refined Iasmin's calculation method. However, multiple absorbance peaks were observed in some bands; therefore, using a single value of absorbance in Iasmin's equation can lead to notable errors. As for acid–base titration, some researchers heated FFAs with excess potassium hydroxide (KOH), which did not participate in saponification [18]. The KOH content remaining after the complete conversion of FFAs into potassium salts was subjected to acid–base titration, and the amount of unreacted FFAs was determined. Based on the findings, the extent of the chemical reaction between FOG deposits and KOH was calculated. However, erroneous results were obtained because the titration end point had to be manually observed, necessitating the development of precise assessment methodologies.

Beyond accurate measurement of saponification extent, understanding the reaction kinetics is essential for predicting how environmental factors influence FOG deposit formation. Accordingly, a kinetic model was developed herein to elucidate the impact of temperature variations on FOG deposit formation. Iasmin et al. [13] previously developed a chemical kinetic model for oil deposit formation using FTIR analysis. However, this model primarily calculated the reaction rates based on mass changes, FTIR analysis also exhibited a high error margin.

Herein, gas chromatography–mass spectrometry (GC–MS) was used to test the saponification extent of FOG deposits. The results of acid–base titration, FTIR spectroscopy and GC–MS were compared to identify the testing methodology exhibiting the lowest error rate. Subsequently, single-factor experiments revealed that FFA species, temperature, pH, FFA:$Ca^{2+}$ mass ratio, and reaction time affect the saponification process, followed by response surface methodology (RSM) to identify the most adverse conditions for FOG deposit formation. Finally, focusing on chemical kinetic mechanisms, the kinetic equations and reaction orders for the saponification reaction between FFAs and $Ca^{2+}$ in FOG deposits were determined. In addition, a chemical kinetic model for FOG deposit formation was developed based on reaction temperature variations to establish a theoretical foundation for exploring the formation mechanisms of FOG deposits. Overall, the findings provide critical insights into optimizing the strategies for FOG deposit removal and enhancing the current operational management of kitchen drainage systems.

## 2. Materials and Methods

### 2.1. Chemical Reagents and Equipment

1% phenolphthalein (a pH indicator solution), a 0.5000 $mol \cdot L^{-1}$ KOH standard titration solution and a 0.5000 $mol \cdot L^{-1}$ HCl standard titration solution were purchased from Guangzhou Howei Pharma Tech Co., Ltd. (Guangzhou, China). Lauric acid ($C_{12}H_{24}O_2$), myristic acid ($C_{14}H_{28}O_2$), $C_{16}H_{32}O_2$ and $C_{18}H_{34}O_2$ were purchased from Aladdin Reagent Co., Ltd. (Shanghai, China). $CaCl_2$ and sodium hydroxide (NaOH) were purchased from Sinopharm Chemical Reagent Co., Ltd. (Shanghai). All chemicals and reagents were directly used as received without further purification, and the

experimental solutions were prepared using deoxygenated ultrapure water (electrical resistivity: 18.25 MΩ·cm at 25°C) as the solvent. An SB-5200D ultrasonic cleaner manufactured by Ningbo Scientz Biotechnology Co., Ltd. (Ningbo, China) as well as an LC-DMS-H constant-temperature magnetic stirrer and a PH-100 Pro electric thermometer manufactured by Shanghai Lichen Instrument Technology Co. Ltd. (Shanghai, China) were used.

## 2.2. Testing Method Principles

### 2.2.1. FTIR Analysis and Acid–Base Titration

To determine the saponification extent, the mass ratio of fatty acid calcium derived from the saponification of FOG deposits relative to the total FOG deposits was calculated (denoted as *R*, %). Higher *R* values indicated a greater saponification extent of FOG deposits. Del et al.'s FTIR method was used to determine the saponification extent and the corresponding formula [7, 16], and the acid–base titration method reported by Mahesar et al. and Wang et al. was also employed in this research [19, 20].

### 2.2.2. GC–MS

The amounts of FFAs and $Ca^{2+}$ participating in FOG deposit formation were identified from the FOG formation principle. Assuming that the total amount of FFAs is $A + B$ (known), the amount involved in its saponification reaction with $Ca^{2+}$ into fatty acid calcium is $A$ and the amount of physical deposition is $B$. Then, the amount of $B$ can be quantitatively determined via GC–MS. The saponification extent can be calculated as follows:

$$\text{Saponification extent } (\%) = \left(1 - \frac{A}{A+B}\right) \times 100\% \quad (1)$$

The peak area of unreacted FFAs in the experimental product (total mass *M*) was determined via peak area normalisation and denoted as *b*. The FFA species (C) were identified by matching their mass spectra to those in a reference database. The peak area of pure compound C with the same mass *M* was measured under identical GC–MS conditions using the same normalisation method, with the corresponding value denoted as *a*. The saponification extent of FOG deposits was then calculated as follows:

$$R(\%) = \left(1 - \frac{b}{a}\right) \times 100\% \quad (2)$$

The specific testing methods are the same as those in the study by Yan et al. [21].

### 2.2.3. Accuracy Test

The accuracy of FTIR, acid–base titration, and GC–MS methods was analyzed using mixed samples containing $C_{18}H_{34}O_2$ and $CaCl_2$ with pre-defined and known saponification extent of FOG deposits. Each sample group was measured five times, and their extent of saponification was calculated. The obtained values were compared to identify the best method. The mixing ratios and experimental conditions are summarized in Table 1.

**Table 1. Experimental conditions of M1–M9 and saponification extents**

| Conditions | Total mass (g) | $C_{18}H_{34}O_2$ (g) | $CaCl_2$ (g) | Extent of Reaction (%) |
|---|---|---|---|---|
| M1 | 1.0 | 0.1 | 0.9 | 10 |
| M2 | 1.0 | 0.2 | 0.8 | 20 |
| M3 | 1.0 | 0.3 | 0.7 | 30 |
| M4 | 1.0 | 0.4 | 0.6 | 40 |
| M5 | 1.0 | 0.5 | 0.5 | 50 |
| M6 | 1.0 | 0.6 | 0.4 | 60 |
| M7 | 1.0 | 0.7 | 0.3 | 70 |
| M8 | 1.0 | 0.8 | 0.2 | 80 |
| M9 | 1.0 | 0.9 | 0.1 | 90 |

## 2.3. Influencing Factors

### 2.3.1. Single-Factor Experiment

The influence of five factors, reaction temperature, pH, FFA species, FFA:$Ca^{2+}$ mass ratio, and reaction duration, on the saponification extent of FOG deposits was determined via single-factor experiments. The process is shown in Figure 1. First, 1.0000 g of the FFA was precisely measured and dissolved in 9.0 mL of $C_2H_5OH$. A pre-determined

mass of $CaCl_2$ was quantitatively dissolved in 1.00 mL of deoxygenated ultrapure water, and its pH was adjusted using 0.5000 mol·L$^{-1}$ of the KOH standard titration solution. The solution was then transferred to a round-bottom flask mounted on a constant-temperature magnetic stirrer. The temperature probe of the stirrer was immersed in the solution, and the stirring temperature and time were set to pre-determined values. After the completion of stirring, the mixture was transferred from the flask to a high-speed centrifuge and centrifuged for 5 min. Then, 0.1000 mL of the supernatant was transferred to the GC–MS system to determine the FFA species. The saponification extent of FOG deposits was determined under the above-mentioned conditions by quantitatively measuring the peak area corresponding to the unreacted FFAs. To this end, 1.0000 g of a purified FFA compound obtained via qualitative analysis was dissolved in 10.0 mL of $C_2H_5OH$. This solution was then centrifuged at a high speed for 5 min, after which the supernatant was subjected to GC–MS analysis; this solution served as the analytical and calibration standard. Finally, the peak area of the calibration standard was measured and comparatively analyzed with that of unreacted FFAs to determine the saponification extent of FOG deposits under different single-factor conditions. All experimental procedures were performed five times, and the arithmetic mean values were used for final calculations and results.

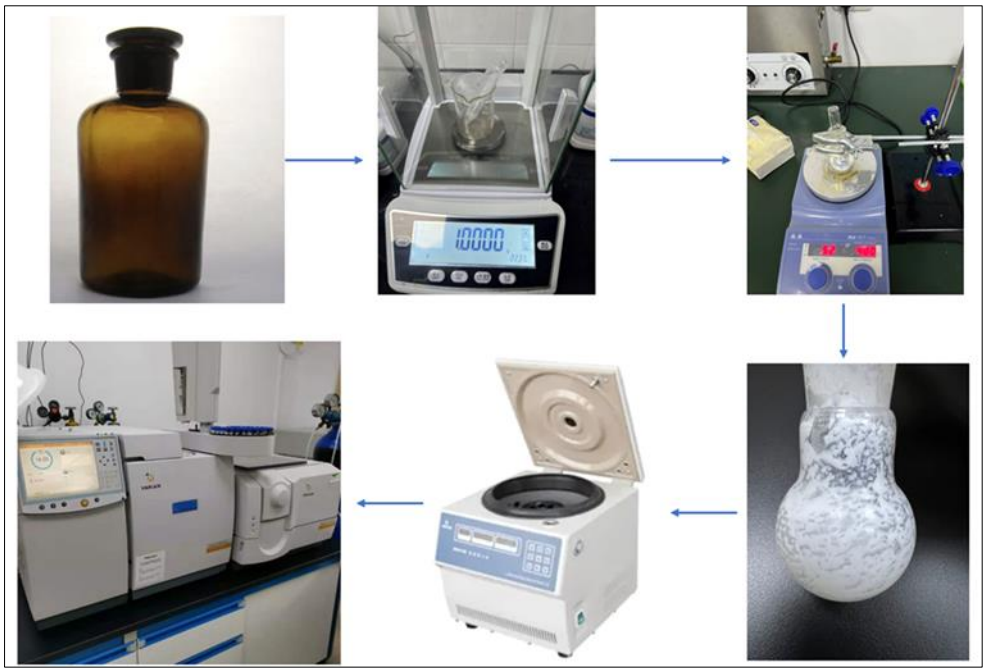

**Figure 1. Procedure of single-factor experimental test**

### 2.3.2. Influence Degree of Different Factors

A central composite design (CCD) was developed using Design-Expert® 13 software based on the ranges of the aforementioned five factors to quantify their influence degree on the saponification extent of FOG deposits. The saponification reaction conditions were then optimized through experiments similar to the single-factor experiments.

## 2.4. Chemical Kinetic Model

### 2.4.1. Reaction Rate Equation of Saponification

Under certain experimental conditions, wherein all side reactions are considered negligible, the apparent reaction rate ($r$) for saponification between FFA and $Ca^{2+}$ can be calculated as follows:

$$r = \frac{dC_{FFA}}{dt} = kC_{FFA}^{m}C_{Ca^{2+}}^{n} \quad (3)$$

where $k$ is the apparent reaction rate constant (mol·L$^{-1}$·min$^{-1}$), $C_{FFA}$ is the molar concentration of FFA at time point $t$ (mol·L$^{-1}$), $C_{Ca^{2+}}$ is the molar concentration of $Ca^{2+}$ at time point $t$ (mol·L$^{-1}$), $t$ is the reaction duration (min) and $m$ and $n$ are the experimentally derived reaction orders for FFA and $Ca^{2+}$, respectively.

### 2.4.2. Deduction of Reaction Orders

FFA and $Ca^{2+}$ were proportioned according to the stoichiometric ratio for saponification; that is, their initial concentrations (at $t$ = 0 min) satisfied the following relation:

$$C_{Ca^{2+}|t=0} = \frac{1}{2}C_{FFA|t=0} \quad (4)$$

At time point *t*, the saponification extent is *R* (%) and the corresponding FFA concentration is:

$$C_{\mathrm{FFA}} = C_{\mathrm{FFA}|t=0}(1-R) \tag{5}$$

Correspondingly, $Ca^{2+}$ concentration at time point *t* becomes:

$$C_{\mathrm{Ca^{2+}}} = C_{\mathrm{Ca^{2+}}|t=0} - \frac{1}{2}C_{\mathrm{FFA}|t=0}R = \frac{1}{2}C_{\mathrm{FFA}|t=0}(1-R) = \frac{1}{2}C_{\mathrm{FFA}} \tag{6}$$

Substituting Equation 6 into Equation 3 reduces the kinetic formulation to:

$$r = \frac{dC_{\mathrm{FFA}}}{dt} = kC_{\mathrm{FFA}}^{m}C_{\mathrm{Ca^{2+}}}^{n} = kC_{\mathrm{FFA}}^{m}(\frac{1}{2}C_{\mathrm{Ca^{2+}}})^{n} = k(\frac{1}{2})^{n}C_{\mathrm{FFA}}^{m+n} \tag{7}$$

Defining $k' = k(\frac{1}{2})^{n}$ and substituting it into Equation 7 yields:

$$r = k(\frac{1}{2})^{n}C_{\mathrm{FFA}}^{m+n} = k'C_{\mathrm{FFA}}^{m+n} = k(\frac{1}{2})^{m-1}C_{\mathrm{FFA}}^{m+n} \tag{8}$$

Taking the logarithm of both sides of Equation 8 yields:

$$ln\, r = ln\, k' + ln(\,C_{\mathrm{FFA}}^{m+n}) = ln\, k' + (m+n)\, ln(\,C_{\mathrm{FFA}}) = ln(-\frac{dC_{\mathrm{FFA}}}{dt}) \tag{9}$$

The overall reaction order $(m+n)$ for FFA and $Ca^{2+}$ was derived from the $ln(-\frac{dC_{\mathrm{FFA}}}{dt})$–$ln(\,C_{\mathrm{FFA}})$ relation curve, and the individual reaction orders *m* and *n* were determined, respectively, based on the influence degree of each factor in the single-factor experiments.

### 2.4.3. Deduction of Apparent Reaction Rate Constant (*k*)

As $m+n \neq 1$, i.e. saponification did not follow first-order kinetics, *k* was derived based on the rate laws of second-order and higher-order kinetic reactions

$$\int_{C_{\mathrm{FFA}|t=0}}^{C_{\mathrm{FFA}}} -\frac{dC_{\mathrm{FFA}}}{dC_{\mathrm{FFA}}^{m+n}} = \int_{0}^{t} k'\,dt \tag{10}$$

$$\frac{1}{m+n-1} \times C_{\mathrm{FFA}}^{1-(m+n)} \Big|_{C_{\mathrm{FFA}|t=0}}^{C_{\mathrm{FFA}}} = k't \tag{11}$$

$$C_{\mathrm{FFA}}^{1-(m+n)} = (m+n)k't + \frac{1}{m+n-1} \times C_{\mathrm{FFA}|t=0}^{1-(m+n)} \tag{12}$$

As $k' = k(\frac{1}{2})^{n} = k(\frac{1}{2})^{m-1}$, *k* was deduced accordingly.

### 2.4.4. Deduction of Activation Energy ($E_a$, kJ·mol$^{-1}$)

$E_a$ is the energy required for molecules to transform from normal state to an activated state that is conducive to chemical reactions. It is the minimum energy required to initiate a chemical reaction. Based on the indefinite integral expression of Arrhenius equation, it can be deduced that

$$k = A \cdot e^{-\frac{E_a}{RT}} \tag{13}$$

Taking the logarithm of both sides of Equation 13 yields

$$ln\, k = ln\, A - \frac{E_a}{R} \times \frac{1}{T} \tag{14}$$

where *T* is the thermodynamic temperature (K), *A* is the pre-exponential factor, with the same units as the concentration–based apparent reaction rate constant *k* (mol·L$^{-1}$·min$^{-1}$ in this study), and *R* is the molar gas constant, *R* = 8.314 J·mol$^{-1}$·K$^{-1}$.

Then, the relation curve between $ln\, k$ and $\frac{1}{T}$ was plotted, with $-\frac{E_a}{R}$ as the slope. The intercept was $ln\, A$, from which $E_a$ and *A* were calculated.

## 3. Results and Discussion

### 3.1. Comparative Evaluation of Testing Methods

Working conditions M1–M9 were systematically evaluated using acid–base titration, FTIR, and GC–MS methods. The obtained results (Figure 2) were compared with the saponification extent obtained under actual operating conditions, and the corresponding error rates were calculated. The standard deviations were less than 5% of the means across all measurements, demonstrating good reproducibility. The GC–MS results closely matched the pre-determined

saponification extent under actual operating conditions, whereas the FTIR results exhibited considerably poor accuracy. The mean error rates determined by comparing measured and theoretical values were 8.7%, 16.1%, and 47.9% for GC–MS, acid–base titration, and FTIR analyses, respectively.

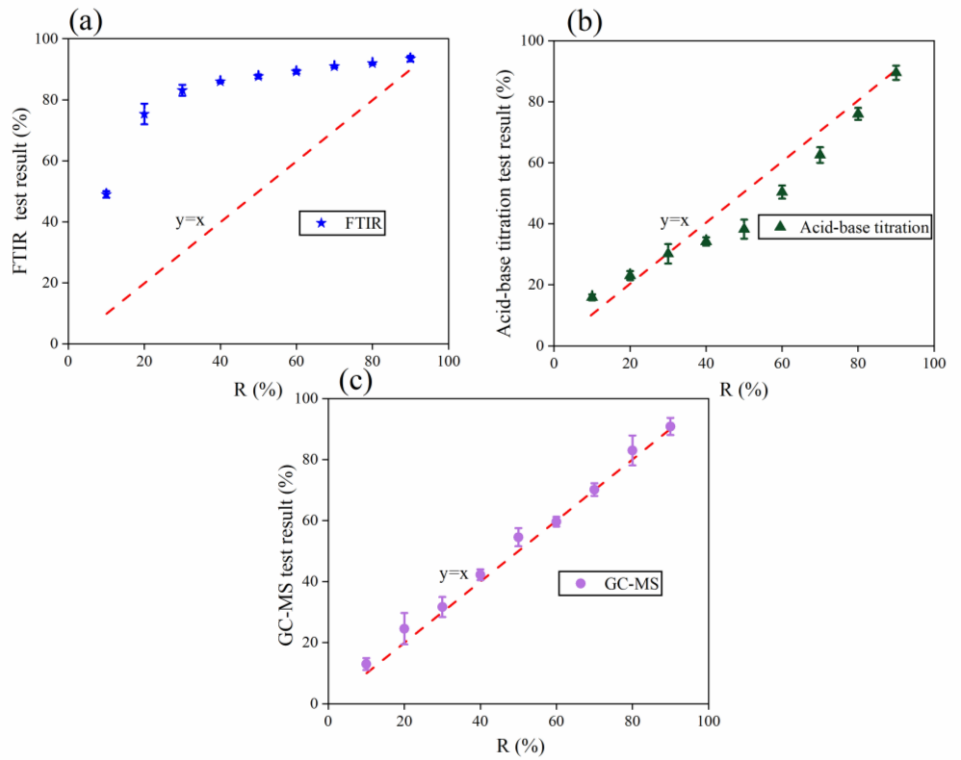


**Figure 2. Testing methods for saponification extent of FOG deposits: (a) FTIR; (b) Acid-Base titration; (c) GC-MS.**

FTIR measurements exhibited a considerably higher mean error rate due to methodological constraints associated with the KBr grinding–pressing disc method. Insufficient grinding of samples with KBr induced light scattering and baseline drift during spectral acquisition [22, 23]. Random sample sizes during disc pressing generated inconsistent thicknesses, leading to interference fringes in the FTIR spectra for thicker discs. Pressure and duration during disc pressing could not be precisely regulated, resulting in over-compaction of discs and considerable surface smoothening [24], which in turn caused light polarization and the appearance of anomalous high-intensity sharp spectral peaks. The inherent resolution limitations of conventional FTIR spectrometers, combined with operational constraints, fundamentally reduced measurement accuracy.

The errors in the acid–base titration method primarily originated from the manual judgment inaccuracy of the titration endpoint and color, resulting in an error in the titration volume [25, 26]. Meanwhile, acid–base titration yielded acceptable accuracy levels and had simple operation [27].

GC–MS showed the lowest error rate and was therefore deemed the optimal method for determining the saponification extent of FOG deposits in terms of accuracy. Recent studies have shown that GC–MS exhibits high sensitivity for detecting and identifying FFA across multiple scenarios, including solid and liquid phases [28-30]. Vasiliki et al. [31] reported that GC–MS enables rapid and robust quantification of short‐chain fatty acids in solid–liquid mixed phases, achieving a response rate exceeding 95.5% for four-carbon FFAs with an error rate below 5.0%. However, its operating procedure is extensive and complex, rendering the calibration process expensive. In addition, the requirement of pure standards adds to the high testing cost. Thus, this method is recommended only for scenarios that demand high-precision results, whereas for routine applications, acid–base titration may be a more practical choice despite its moderate error rate.

## 3.2. Parameter Ranges of Factors

### 3.2.1. FFAs Species

FFAs in FOG deposits from kitchen drainage pipes mainly contain compounds such as $C_{12}H_{24}O_2$, $C_{14}H_{28}O_2$, $C_{16}H_{32}O_2$ and $C_{18}H_{34}O_2$. As a preliminary basis before investigating other factors, the experimental parameters were set as follows: FFA and $CaCl_2$ masses of 1.0 and 1.4 g (mass ratio of 1.4), respectively, pH value of 5, temperature of 30°C and reaction duration of 60 min. The saponification extent of FOG deposits for each FFA was determined via GC–MS (Figure 3).

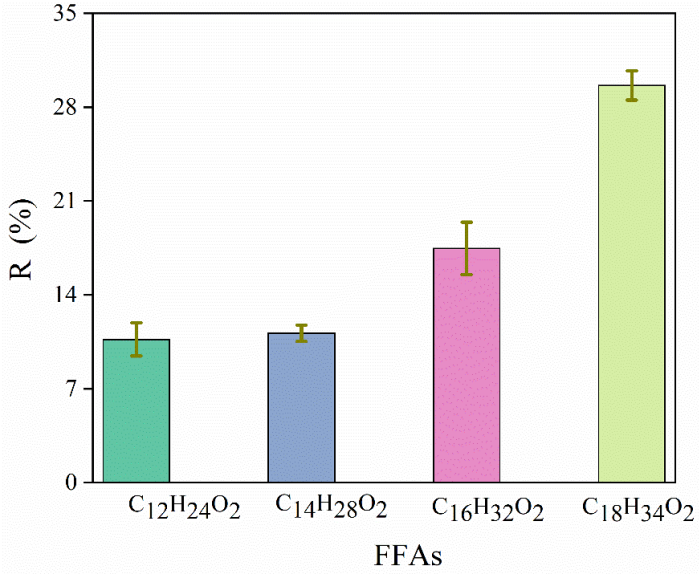


**Figure 3. Effect of FFAs species on saponification extent of FOG deposits**

As shown in Figure 3, amongst the four common FFAs ($C_{12}H_{24}O_2$, $C_{14}H_{28}O_2$, $C_{16}H_{32}O_2$ and $C_{18}H_{34}O_2$) tested under identical conditions, $C_{18}H_{34}O_2$ exhibited the highest saponification extent. This finding is consistent with previous reports indicating that fats with higher oleic acid ratios produce calcium saponified solids with greater yield and saponification extent. During the nucleophilic substitution reaction in saponification, the carbonyl carbon of acyl group acted as the reactive site and played the leading role. When the FFA mass was kept constant at 1.0 g, their relative molecular mass increased with increasing number of carbon atoms in its chain. When 1.0 g of pure $C_{12}H_{24}O_2$, $C_{14}H_{28}O_2$, $C_{16}H_{32}O_2$ and $C_{18}H_{34}O_2$ were used, the masses of their carbonyl group were 0.14, 0.12, 0.11 and 0.09 g, respectively. $C_{18}H_{34}O_2$ exhibited the highest relative molecular mass, resulting in a lower mass contribution from the carbonyl carbon atom in the acyl group compared with $C_{12}H_{24}O_2$, $C_{14}H_{28}O_2$ and $C_{16}H_{32}O_2$ [32]. Therefore, it was more susceptible to nucleophilic attack by hydroxide ions ($OH^-$) due to its lower steric hindrance at the carbonyl carbon, generating abundant negatively charged intermediates and increasing the saponification extent of its FOG deposits. The difference in the reaction extent of FFAs was influenced by their solubility in kitchen wastewater. $C_{18}H_{34}O_2$ was more soluble compared with other FFAs, yielding a greater saponification extent of FOG deposits. Notably, this study employed $C_{18}H_{34}O_2$ as the sole model FFA to investigate the saponification kinetics of FOG deposits. However, in real kitchen wastewater, FFAs exist as a mixture rather than a single component. The presence of less reactive FFAs, such as $C_{12}H_{24}O_2$, $C_{14}H_{28}O_2$ and $C_{16}H_{32}O_2$, which showed lower saponification extents than $C_{18}H_{34}O_2$ in our experiments, likely reduces the overall saponification extent in mixed systems. Consequently, the actual FOG deposit formation may be lower than the values predicted by the saponification reaction calibrated using pure $C_{18}H_{34}O_2$.

### 3.2.2. Mass Ratio

Different mass ratios were obtained by keeping the mass of $C_{18}H_{34}O_2$ constant at 1.0 g and changing the mass of $CaCl_2$ as 1:0.10, 1:0.20, 1:0.50, 1:1.00, 1:1.20, 1:1.40 and 1:1.59; their influence on the saponification extent of the resulting FOG deposits was tested at a pH value of 5, temperature of 30°C and reaction duration of 60 min. Notably, a $C_{18}H_{34}O_2$:$CaCl_2$ mass ratio of 1:1.59 was defined as the threshold because the solubility of $CaCl_2$ in 100 g water was ≤159 g at standard pressure and 30°C, i.e. it reached its saturation limit under these controlled conditions.

As shown in Figure 4-a, the saponification extent of FOG deposits from $C_{18}H_{34}O_2$ increased with increasing $CaCl_2$ mass and reached equilibrium at approximately 25%, corresponding to a $C_{18}H_{34}O_2$:$CaCl_2$mass ratio of 1:1.40. According to the chemical reaction equation between FFAs and $Ca^{2+}$ (Equation 4), the $C_{18}H_{34}O_2$:$CaCl_2$ molar ratio is 2:1. Converting these into mass, 1.0 g of $C_{18}H_{34}O_2$ corresponded to approximately 0.2 g of $CaCl_2$. In other words, when the $C_{18}H_{34}O_2$:$CaCl_2$ mass ratio was 1:0.2, the reaction between them proceeded to completion. Results showed that at a $C_{18}H_{34}O_2$:$CaCl_2$ mass ratio of 1:0.2, $CaCl_2$ was completely dissolved; however, the reaction extent was low. The reaction extent between FFAs and $Ca^{2+}$ increased with increasing $CaCl_2$ mass; however, it did not increase considerably beyond a $C_{18}H_{34}O_2$:$CaCl_2$ mass ratio of 1:1.40. This indicated that $CaCl_2$ mass was no longer a limiting factor for the saponification extent. An explanation for this optimal ratio can be proposed based on the dual role of $Ca^{2+}$. At low $Ca^{2+}$ concentrations, the saponification reaction is limited by $Ca^{2+}$ availability. As the $Ca^{2+}$ concentration is increased, it supplies more reactant and exerts two promoting effects. First, $Ca^{2+}$ compresses the electrical double layer surrounding FFA micelles, thereby facilitating FFA deprotonation and subsequent saponification. Second, $Ca^{2+}$ neutralises negatively charged reaction intermediates, promoting calcium soap precipitation and driving the reaction equilibrium

forward. However, when the $Ca^{2+}$ concentration exceeds the optimal level (i.e. beyond the 1:1.40 mass ratio), inhibitory effects begin to dominate. Excess $Ca^{2+}$ may competitively consume hydroxide ions ($OH^-$) through $Ca(OH)^+$ or $Ca(OH)_2$ precipitate formation. In addition, excessive $Ca^{2+}$ can result in saturated adsorption on the surface of FFA droplets, physically blocking further reaction. Thus, the 1:1.40 ratio represents a balance between the promoting and inhibitory effects of $Ca^{2+}$. Herein, subsequent single-factor experiments were conducted at a $C_{18}H_{34}O_2$:$CaCl_2$ mass ratio of 1:1.40.

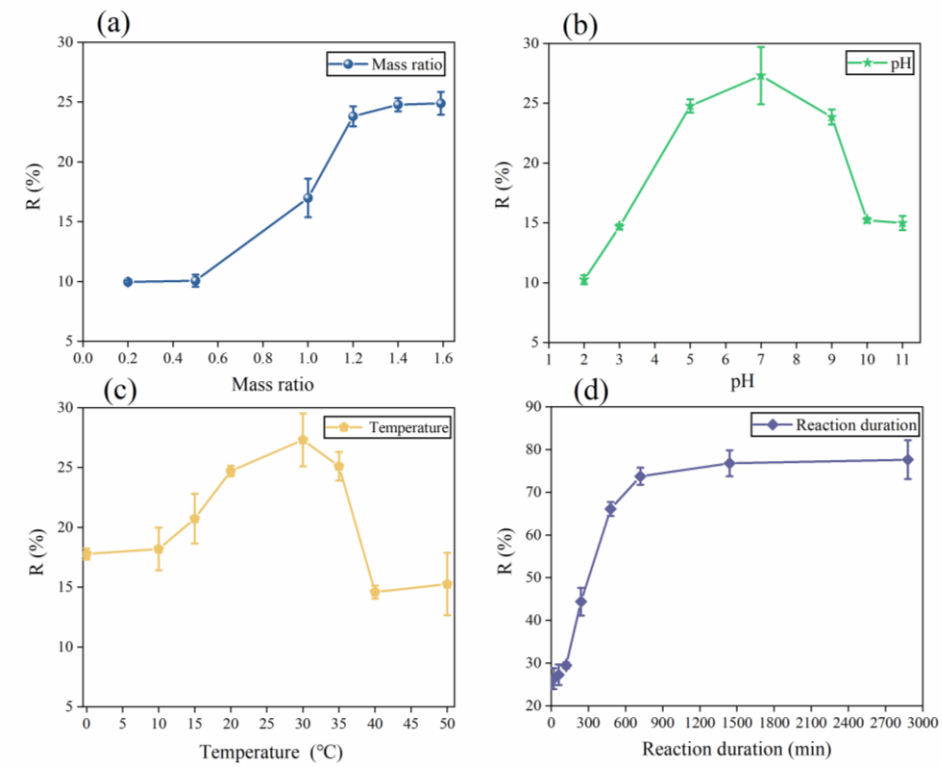


**Figure 4. Factors on fatty acid calcium ($C_{18}H_{34}O_2$) production: (a) $C_{18}H_{34}O_2$:$CaCl_2$ mass ratio; (b) pH; (c) temperature; (d) reaction duration**

### 3.2.3. pH

Highly acidic (pH < 3) or alkaline (pH > 10) cleaning agents are generally used for the unblocking and maintenance of kitchen drainage pipes. To simulate realistic pipe maintenance scenarios where pH extremes may occur, the saponification extent of FOG deposits was tested at a wide pH range of 2–11 (2, 3, 5, 7, 9, 10 and 11) and other parameters were fixed as follows: $C_{18}H_{34}O_2$:$CaCl_2$ mass ratio of 1:1.40, reaction temperature of 30°C and reaction duration of 60 min.

Figure 4-b shows that the saponification extent of FOG deposits first increased with increasing pH, reached a maximum at pH 7 and then decreased. This behavior can be explained as follows. The reaction mechanism between FFAs and $Ca^{2+}$ determines the differences in FFA hydrolysis pathways under different pH conditions. Under acidic aqueous conditions, FFAs hydrolysis is primarily mediated by the nucleophilic reaction between FFAs and a nucleophile derived from $OH^-$ of water molecules ($H_2O$). Under alkaline aqueous conditions, alkaline reagents mainly provide nucleophiles to promote FFA hydrolysis. Under neutral conditions, abundant nucleophiles simultaneously originate from both the alkaline reagents and $H_2O$-derived $OH^-$. As a result, the nucleophilic activity is enhanced and nucleophilic addition reactions easily occur. Consequently, the saponification extent increases to its maximum at pH 7. Ulfa & Eka Cahyani [33] stated that pH influences the solubility of Ca and that $Ca^{2+}$ may start combining with FFAs under neutral conditions. Gomes et al. [34] argued that a higher saponification extent under neutral conditions is attributed to the relative chemical stability of fatty acid calcium salts under neutral or alkaline conditions, whereas these salts degrade under acidic conditions, releasing FFAs and $Ca^{2+}$. The subsequent single−factor experiments were conducted at pH 7 [35, 36].

### 3.2.4. Temperature

The saponification extent of FOG deposits was investigated by varying the reaction temperature (0°C, 10°C, 15°C, 20°C, 30°C, 40°C and 50°C) while keeping other parameters constant: $C_{18}H_{34}O_2$:$CaCl_2$ mass ratio of 1:1.40, pH value of 7 and reaction duration of 60 min. The minimum temperature was set to 0°C because the minimum operating temperature limit of the GC–MS instrument was 0°C. In addition, $C_{18}H_{34}O_2$ might gradually solidify at extremely low

temperatures, physically kinetically limiting the production of fatty acid calcium salts. The maximum temperature was set to 50°C for two reasons. First, in GC–MS testing, $C_2H_5OH$ was selected as the solvent. When the temperature exceeded 50°C, extraneous peaks and ghost peaks corresponding to $C_2H_5OH$ emerged, compromising the measurement of the final target peak areas. Second, in practical engineering, the flow path of kitchen wastewater is as follows: from floor drains into kitchen drainage pipes, sequentially passing through traps, horizontal branch pipes, vertical pipes, and elbows, and finally entering kitchen horizontal main pipes [37, 38]. Under such conditions, the wastewater temperature generally does not exceed 50°C. These findings indicate that the set temperature range of 0°C–50°C was ideal.

Figure 4-c shows that the saponification extent of FOG deposits increased with temperature within the 0°C–30°C range, reaching its maximum at 30°C. However, the saponification extent decreased in the 30°C–50°C range, indicating that elevated temperatures may inhibit saponification. These results contradict previous studies suggesting that higher temperatures enhance FOG formation. FFA hydrolysis behaves as a reversible endothermic reaction under neutral conditions, where increasing temperature increases the number of active molecules in reactants, intensifies Brownian motion, accelerates molecular migration rates, and promotes $OH^-$ release, thereby increasing reaction efficiency [39]. However, these conclusions were based on limited temperature comparisons, as the experiments were conducted only at 22°C and 45°C, restricting the generality of their findings. Meanwhile, this study investigated a continuous temperature range (0°C–50°C), allowing for a more comprehensive evaluation of temperature effects. When temperature exceeded the set threshold, excessive heat easily induced the decomposition and disruption of ionic bonds in fatty acid calcium salts. $C_{18}H_{34}O_2$ has a melting point of 13°C–14°C. It progressively melted as the temperature was increased from 0°C to 30°C, undergoing a solid–liquid phase transition. As a result, excessive amounts of C18H34O2 participated in saponification and increased the saponification extent, peaking at 30°C [40]. Beyond 30°C, the bonds between $Ca^{2+}$ and FFAs in fatty acid calcium salts are disrupted, and the saponification extent decreases [41]. Temperature substantially influenced the Brownian motion, causing variations in the diameter of $C_{18}H_{34}O_2$ molecules. The Brownian motion of $C_{18}H_{34}O_2$ molecules was suppressed at considerably low water temperatures. With increasing temperature, the diffusion rate of molecules accelerated, and intermolecular motion became more vigorous. Under these conditions, $C_{18}H_{34}O_2$ molecules aggregated into small molecular clusters and formed droplet-like structures that encapsulated $Ca^{2+}$ and underwent reactions to yield fatty acid calcium salts. Beyond the optimal temperature range, $C_{18}H_{34}O_2$ molecules further aggregated into smaller droplet-like structures owing to their expanded molecular distance. They thus failed to encapsulate $Ca^{2+}$ and inhibited the formation of fatty acid calcium salts, decreasing the saponification extent of FOG deposits. Subsequent single-factor influence experiments were conducted at a temperature of 30°C.

### 3.2.5. Reaction Duration

The saponification extent of FOG deposits was investigated at a wide reaction duration range of 0–2880 min (0, 18, 60, 120, 240, 480, 720, 1440, and 2880 min), and other parameters were fixed as follows: $C_{18}H_{34}O_2$ :$CaCl_2$ mass ratio of 1:1.40, pH value of 7, and reaction temperature of 30°C. Figure 4-d shows that from the 120th min, the saponification extent of FOG deposits continuously increased and reached equilibrium at the 1440th min; at this point, the saponification extent approached 77%. This indicated that prolonged reaction duration enabled FFAs to react with more $Ca^{2+}$ , thereby generating fatty acid calcium salts. Although saponification was essentially completed by 1440 min, the extent only reached 77.23%, far below the theoretically maximum extent of 100%. This phenomenon indicated that pH, temperature, and reactant mass ratio still hindered saponification. Therefore, further experiments are required to identify more unfavorable working conditions to explore a higher saponification extent.

## 3.3. Influence Ranking of Single Factors

The single-factor experiment revealed the ideal parameters as a $C_{18}H_{34}O_2$:$CaCl_2$ mass ratio of 1:1.40, pH value of 7, reaction temperature of 30°C, and reaction duration of 1440 min. An orthogonal test of these four factors and five levels was designed based on the RSM, and the step sizes were set as 240 min for reaction duration, 0.2 for mass ratio, 2 units for pH, and 10°C for reaction temperature. The level codes and test operation values of each factor are shown in Table 2. Notably, FFA species were not considered a factor because $C_{18}H_{34}O_2$ exhibited the highest saponification rate.

**Table 2. Level codes and test operation values of each factor**

| Levels | Factors | | | |
|---|---|---|---|---|
| | A-Duration | B-Mass ratio | C-pH | D-Temperature |
| -2 | 480 | 1.0 | 3 | 10 |
| -1 | 720 | 1.2 | 5 | 20 |
| 0 | 960 | 1.4 | 7 | 30 |
| 1 | 1200 | 1.6 | 9 | 40 |
| 2 | 1440 | 1.8 | 11 | 50 |

To analyze the combined effects of these factors on the saponification extent of FOG deposits, multifactor experiments were designed as follows. First, the RSM was applied to quantify the influencing degree of each factor, and all numerical results were subjected to curve fitting to derive a predictive equation. RSM analysis was then performed to evaluate the interactions between factors and a regression model was developed correlating all influencing factors with the saponification extent. Finally, the model was validated, and the factors were ranked based on their quantified impact degrees.

### 3.3.1. Establishment and Analysis of Regression Model

RSM analysis results are shown in Table 3. The model design comprised 30 experimental running points, with points 25–30 serving as central points to assess the experimental errors observed during simultaneously repeated experiments. The data were fitted by CCD using the Design-Expert 10.0.3 software, and a regression equation was established, with the saponification extent ($R$ (%)) as the dependent variable and the influencing factors as independent variables as follows:

$$R(\%) = 74.73 + 1.26 \times A + 3.19 \times B - 0.53 \times C - 9.7 \times D - 0.38 \times AB + 0.31 \times AC + 0.89 \times AD - 0.14 \times BC - 0.067 \times BD + 1.12 \times CD - 1.06 \times A^2 - 3.83 \times B^2 - 9.7 \times C^2 - 9.84 \times D^2 \quad (15)$$

**Table 3. Starpoint design results for effect surfaces**

| Number | A-duration | B-ratio | C-pH | D-temperature | $R$(%) |
|---|---|---|---|---|---|
| 1 | 720 | 1.2 | 5 | 20 | 59.7 |
| 2 | 1200 | 1.2 | 5 | 20 | 59.0 |
| 3 | 720 | 1.6 | 5 | 20 | 65.7 |
| 4 | 1200 | 1.6 | 5 | 20 | 64.1 |
| 5 | 720 | 1.2 | 9 | 20 | 54.5 |
| 6 | 1200 | 1.2 | 9 | 20 | 56.7 |
| 7 | 720 | 1.6 | 9 | 20 | 62.4 |
| 8 | 1200 | 1.6 | 9 | 20 | 61.7 |
| 9 | 720 | 1.2 | 5 | 40 | 33.5 |
| 10 | 1200 | 1.2 | 5 | 40 | 38.8 |
| 11 | 720 | 1.6 | 5 | 40 | 42.4 |
| 12 | 1200 | 1.6 | 5 | 40 | 43.3 |
| 13 | 720 | 1.2 | 9 | 40 | 37.1 |
| 14 | 1200 | 1.2 | 9 | 40 | 39.5 |
| 15 | 720 | 1.6 | 9 | 40 | 40.7 |
| 16 | 1200 | 1.6 | 9 | 40 | 45.5 |
| 17 | 480 | 1.4 | 7 | 30 | 66.1 |
| 18 | 1440 | 1.4 | 7 | 30 | 74.9 |
| 19 | 960 | 1 | 7 | 30 | 52.0 |
| 20 | 960 | 1.8 | 7 | 30 | 66.8 |
| 21 | 960 | 1.4 | 3 | 30 | 37.0 |
| 22 | 960 | 1.4 | 11 | 30 | 34.9 |
| 23 | 960 | 1.4 | 7 | 10 | 52.9 |
| 24 | 960 | 1.4 | 7 | 50 | 17.9 |
| 25 | 960 | 1.4 | 7 | 30 | 74.5 |
| 26 | 960 | 1.4 | 7 | 30 | 74.6 |
| 27 | 960 | 1.4 | 7 | 30 | 75.4 |
| 28 | 960 | 1.4 | 7 | 30 | 73.4 |
| 29 | 960 | 1.4 | 7 | 30 | 76.2 |
| 30 | 960 | 1.4 | 7 | 30 | 74.2 |

The results of analysis of variance are summarized in Table 4. The model exhibited a high F-value of 205.94 with a P-value of <0.0001. The F-test indicated the significance of the regression equation, thereby demonstrating the reliability of this experimental methodology. Within this model, A, B, D, AD, CD, $A^2$, $B^2$, $C^2$ and $D^2$ were identified as the most influential factors. From this, it could be concluded that the influencing degrees of FFA:$Ca^{2+}$ mass ratio, reaction duration, pH and reaction temperature on saponification extent of FOG deposits were ranked as follows in the descending order: reaction temperature > mass ratio > reaction duration > pH. Amongst these, reaction temperature and mass ratio, with P-values below 0.0001, exhibited the most pronounced effects on the saponification extent. The coefficient of determination ($R^2$) for the regression equation exceeded 0.995, indicating that the derived equation adequately described and evaluated the relations between the factors and response values. The adjusted coefficient of determination (Adj-$R^2$) was 0.9900, greater than 0.8000, and the coefficient of variation was 2.88%; these results demonstrated a good fit of the model, confirming its applicability for preliminary analysis and prediction of FOG deposit formation in process optimization studies.

**Table 4. Analysis of variance results**

| Source of Variation | Sum of Deviation Square | Degrees of Freedom | Sum of Mean Square | F | P | Evaluation of Statistical Significance |
|---|---|---|---|---|---|---|
| Model | 7294.80 | 14 | 521.06 | 205.94 | <0.0001 | ** |
| A | 38.30 | 1 | 38.30 | 15.14 | 0.0014 | ** |
| B | 244.10 | 1 | 244.10 | 96.47 | <0.0001 | ** |
| C | 6.81 | 1 | 6.810 | 2.69 | 0.1218 | |
| D | 2260.49 | 1 | 2260.49 | 893.4 | <0.0001 | ** |
| AB | 2.31 | 1 | 2.31 | 0.91 | 0.3544 | |
| AC | 1.49 | 1 | 1.49 | 0.59 | 0.455 | |
| AD | 12.57 | 1 | 12.57 | 4.97 | 0.0416 | * |
| BC | 0.33 | 1 | 0.33 | 0.13 | 0.7228 | |
| BD | 0.07 | 1 | 0.07 | 0.029 | 0.8675 | |
| CD | 19.98 | 1 | 19.98 | 7.90 | 0.0132 | * |
| $A^2$ | 30.95 | 1 | 30.95 | 12.23 | 0.0032 | ** |
| $B^2$ | 403.35 | 1 | 403.50 | 159.42 | <0.0001 | ** |
| $C^2$ | 2583.30 | 1 | 2583.30 | 1020.99 | <0.0001 | ** |
| $D^2$ | 2657.03 | 1 | 2657.03 | 1050.12 | <0.0001 | ** |
| Residual | 37.95 | 15 | 2.53 | | | |
| Lack of fit | 33.26 | 10 | 3.33 | 3.54 | 0.0876 | ns |
| Pure error | 4.69 | 5 | 0.94 | | | |
| Sum | 7332.75 | 29 | | | | |
| $R^2$ = 0.9948; Adj$R^2$ = 0.9900; C.V.% = 2.88 | | | | | | |

Note: * means P<0.05 indicating a significant difference; ** means P<0.01 indicating a extremely significant.

### 3.3.2. RSM Analysis

Figure 5 presents the 3D response surface plots created using the regression equation (Equation 15). These plots were used to analyze the interactions between the influencing factors and the shape of the fitted response surface. Factors such as reaction duration, $C_{18}H_{34}O_2$:$CaCl_2$ mass ratio, temperature, and pH that affect the chemical formation of FOG deposits were particularly analyzed, and Figures 5-a to 5-c display their similar variation trends. As revealed by Figure 5-a, the saponification extent of FOG deposits increased with increasing reaction duration and $C_{18}H_{34}O_2$:$CaCl_2$ mass ratios. However, when the $C_{18}H_{34}O_2$:$CaCl_2$ mass ratio exceeded 1:1.40, the saponification extent decreased owing to the poor solubility of $CaCl_2$ in water. As shown in Figures 5-b and 5-c, the saponification extent increased with increasing reaction temperature and reaction duration. However, beyond pH 7 and a temperature of 25°C, the saponification extent decreased. As shown in Figures 5-d to 5-f, the saponification extent of FOG deposits initially increased and subsequently decreased as the values of these paired factors increased. For instance, Figure 5-f shows that below a temperature of 25°C and pH of 7, the saponification extent was positively correlated with both reaction temperature and pH; however, immediately after the temperature exceeding 25°C and pH surpassing 7, the saponification was negatively correlated with these two factors. Furthermore, comparative analysis of the interaction factors revealed that the surfaces shown in Figures 5-c to 5-f presented steeper curvatures, indicating that the interactions between reaction duration and temperature as well as between pH and temperature had pronounced effects on the saponification extent.

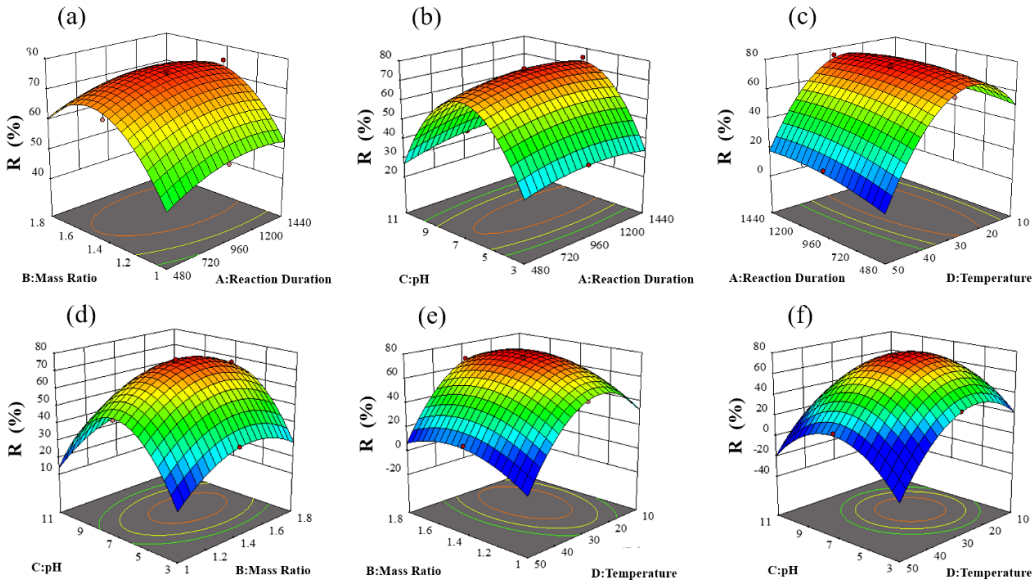


**Figure 5. Interaction of four factors affecting saponification extent of fatty acid calcium: (a) Time VS. Temperature; (b)Time VS. pH; (c) Temperature VS. Time; (d) Mass ratio VS. pH; (e)Temperature VS. Mass ratio; (f) Temperature VS. pH**

### 3.3.3. Verification of the Regression Model

The most unfavorable conditions for the saponification of FOG deposits were predicted based on Equation 15 as follows: reaction duration of 1035.283 min, $C_{18}H_{34}O_2$:$CaCl_2$ mass ratio of 1:1.481, pH value of 6.895 and reaction temperature of 25.170°C. Under these conditions, the maximum saponification extent was predicted to be 77.932%. Five parallel experiments were conducted at a reaction duration of 1036 min, $C_{18}H_{34}O_2$:$CaCl_2$ mass ratio of 1:1.48, pH value of 7 and reaction temperature of 25°C. The average saponification extent of FOG deposits measured via GC–MS was 77.1%, showing a 1.1% deviation from the value predicted by the regression model. The minimal discrepancy between experimental and predicted results demonstrated the validity of the developed model. Therefore, for subsequent reaction kinetics investigations, working conditions were configured with a reaction duration of 1036 min, $C_{18}H_{34}O_2$:$CaCl_2$ mass ratio of 1:1.50, pH value of 7 and reaction temperature of 25°C to enhance the efficiency and accuracy of experimental results.

## 3.4. Chemical Kinetic Model

GC–MS was employed to determine reaction kinetics that governed the formation of fatty acid calcium salts from FFAs and $Ca^{2+}$ under varying reaction temperatures without a catalyst. Based on the four-factor, five-level orthogonal experimental design using the RSM, the most unfavorable temperature for saponification was determined as 25°C. Figure 4-c shows that high reaction rates were achieved at low temperatures. Therefore, the temperature range of 0°C–25°C was selected for analyzing the reaction kinetics herein.

According to the experimental procedures shown in Figure 1, under conditions of 1.0 g of $C_{18}H_{34}O_2$, 1.5 g of $CaCl_2$ and pH 7, the values of the reaction rate constant ($k$) for saponification were determined at 0°C, 10°C, 15°C and 25 °C over a reaction duration of 30–1440 min. The corresponding data are presented in Tables 5 to 8.

**Table 5. Reaction kinetics results at 0℃**

| $t$ (min) | $C_{FFA}$ | $ln(C_{FFA})$ | $-\frac{dC_{FFA}}{dt}$ | $ln(-\frac{dC_{FFA}}{dt})$ | $R$ (%) |
|---|---|---|---|---|---|
| 30 | 0.32 | -1.13 | 6.96E-04 | -7.27 | 8.7 |
| 60 | 0.30 | -1.20 | 4.49E-04 | -7.71 | 14.6 |
| 120 | 0.29 | -1.24 | 1.62E-04 | -8.73 | 18.0 |
| 180 | 0.28 | -1.26 | 1.48E-04 | -8.82 | 20.1 |
| 240 | 0.27 | -1.30 | 2.54E-04 | -8.28 | 23.0 |
| 300 | 0.25 | -1.38 | 2.11E-04 | -8.46 | 28.7 |
| 360 | 0.25 | -1.40 | 9.49E-05 | -9.26 | 30.2 |
| 480 | 0.24 | -1.45 | 1.01E-04 | -9.20 | 33.6 |
| 600 | 0.22 | -1.50 | 8.42E-05 | -9.38 | 37.0 |
| 720 | 0.22 | -1.54 | 4.77E-05 | -9.95 | 39.3 |
| 1200 | 0.20 | -1.60 | 6.46E-05 | -9.65 | 43.1 |
| 1440 | 0.18 | -1.73 | 1.02E-04 | -9.19 | 50.0 |

**Table 6. Reaction kinetics results at 10℃**

| $t$ (min) | $C_{FFA}$ | $ln(C_{FFA})$ | $-\frac{dC_{FFA}}{dt}$ | $ln(-\frac{dC_{FFA}}{dt})$ | $R$ (%) |
|---|---|---|---|---|---|
| 30 | 0.32 | -1.15 | 9.02E-04 | -7.08 | 10.1 |
| 60 | 0.29 | -1.23 | 6.13E-04 | -7.62 | 17.8 |
| 120 | 0.27 | -1.30 | 6.12E-04 | -7.42 | 23.3 |
| 180 | 0.22 | -1.53 | 5.49E-04 | -7.52 | 38.5 |
| 240 | 0.21 | -1.58 | 3.87E-04 | -7.72 | 41.9 |
| 300 | 0.17 | -1.77 | 3.50E-04 | -7.72 | 51.6 |
| 600 | 0.15 | -1.92 | 6.24E-05 | -9.57 | 58.4 |
| 720 | 0.14 | -1.96 | 3.37E-05 | -9.88 | 60.1 |
| 1200 | 0.13 | -2.02 | 2.56E-05 | -10.15 | 62.5 |
| 1440 | 0.13 | -2.08 | 3.36E-05 | -9.53 | 64.8 |
| 600 | 0.15 | -1.92 | 6.24E-05 | -9.57 | 58.4 |
| 720 | 0.14 | -1.96 | 3.37E-05 | -9.88 | 60.1 |

**Table 7. Reaction kinetics results at 15℃**

| $t$ (min) | $C_{FFA}$ | $ln(C_{FFA})$ | $-\frac{dC_{FFA}}{dt}$ | $ln(-\frac{dC_{FFA}}{dt})$ | $R$ (%) |
|---|---|---|---|---|---|
| 30 | 0.31 | -1.18 | 8.45E-04 | -7.08 | 13.6 |
| 60 | 0.28 | -1.27 | 4.92E-04 | -7.62 | 20.7 |
| 120 | 0.27 | -1.30 | 5.98E-04 | -7.42 | 23.1 |
| 180 | 0.21 | -1.57 | 5.42E-04 | -7.52 | 41.0 |
| 240 | 0.21 | -1.57 | 4.45E-04 | -7.72 | 41.5 |
| 300 | 0.16 | -1.86 | 4.45E-04 | -7.72 | 56.1 |
| 360 | 0.15 | -1.87 | 4.86E-05 | -9.93 | 56.5 |
| 480 | 0.15 | -1.93 | 5.56E-05 | -9.80 | 58.9 |
| 600 | 0.14 | -1.96 | 6.95E-05 | -9.57 | 60.3 |
| 720 | 0.13 | -2.05 | 5.12E-05 | -9.88 | 63.6 |
| 1200 | 0.13 | -2.07 | 3.91E-05 | -10.15 | 64.3 |
| 1440 | 0.11 | -2.22 | 7.30E-05 | -9.53 | 69.2 |

**Table 8. Reaction kinetics results at 25℃**

| $t$ (min) | $C_{FFA}$ | $ln(C_{FFA})$ | $-\frac{dC_{FFA}}{dt}$ | $ln(-\frac{dC_{FFA}}{dt})$ | $R$ (%) |
|---|---|---|---|---|---|
| 30 | 0.30 | -1.20 | 1.50E-03 | -6.50 | 14.6 |
| 60 | 0.26 | -1.36 | 8.14E-04 | -7.11 | 27.3 |
| 120 | 0.25 | -1.39 | 2.64E-04 | -8.24 | 29.5 |
| 180 | 0.23 | -1.49 | 4.40E-04 | -7.73 | 36.3 |
| 240 | 0.20 | -1.63 | 6.10E-04 | -7.40 | 44.4 |
| 300 | 0.15 | -1.88 | 5.50E-04 | -7.51 | 56.9 |
| 360 | 0.13 | -2.03 | 2.25E-04 | -8.40 | 63.1 |
| 480 | 0.12 | -2.12 | 1.20E-04 | -9.03 | 66.1 |
| 600 | 0.10 | -2.28 | 1.13E-04 | -9.09 | 71.2 |
| 720 | 0.09 | -2.38 | 4.13E-05 | -10.10 | 73.7 |
| 1200 | 0.09 | -2.41 | 1.88E-05 | -10.88 | 75.7 |
| 1440 | 0.08 | -2.50 | 3.00E-05 | -10.41 | 77.1 |

Based on the saponification extent of FOG deposits at various time points ($t$), the relation curves between $C_{FFA}$ and $t$ were plotted at these four temperatures. The $-\frac{dC_{FFA}}{dt}$ at different time intervals under each temperature was derived from these curves separately (Figure 6-a).

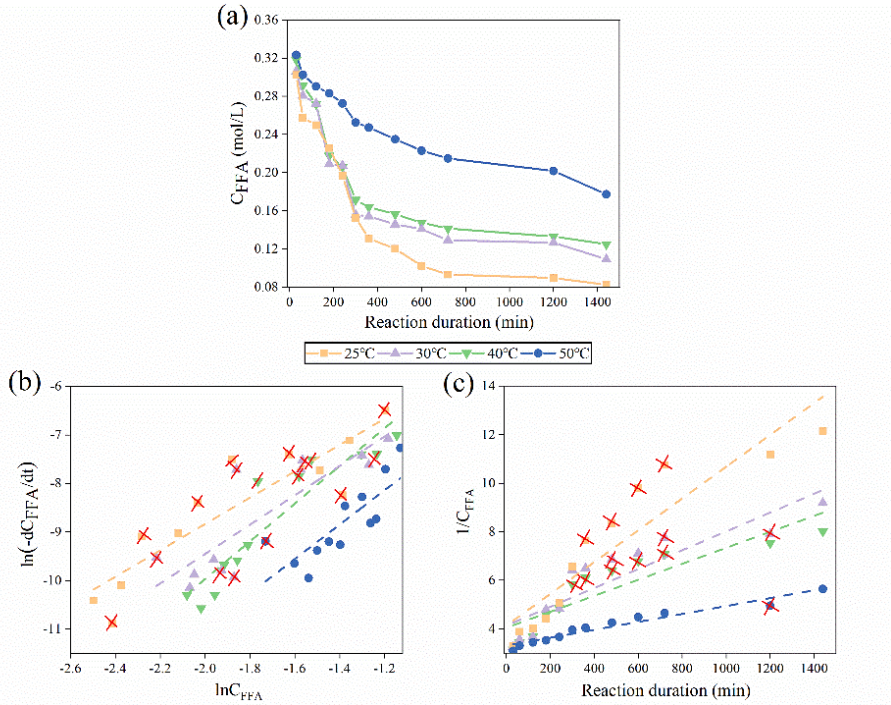


**Figure 6. Kinetic data fitting: (a) $C_{FFA} - t$; (b) $ln(-\frac{dC_{FFA}}{dt}) - ln(C_{FFA})$; (c) $\frac{1}{C_{FFA}} - t$**

The values of $-\frac{dC_{FFA}}{dt}$ at different time points were determined based on the relation between $C_{FFA}$ and $t$. The data were then transformed into logarithmic form to establish the relation between $ln(-\frac{dC_{FFA}}{dt})$ and $ln(C_{FFA})$ (Figure 6-b). Subsequently, linear regression analysis was performed on the data from Figure 6-b. Outlier data points were excluded to ensure that $R^2 \geq 0.9$, and linear fitting equations were obtained for 0°C, 10°C, 15°C and 25°C in Table 9.

**Table 9. Linear fitting equations at four different temperatures**

| Temperature (℃) | Fitting equation | $R^2$ | Slope |
|---|---|---|---|
| 0 | y=2.44x-5.73 | 0.97 | 2.44 |
| 10 | y=2.45x-4.27 | 0.90 | 2.45 |
| 15 | y=2.79x-3.92 | 0.93 | 2.79 |
| 25 | y=2.75x-3.15 | 0.91 | 2.75 |

The slopes of these four lines were all approximately 2, indicating that the chemical reaction satisfied $m + n = 2$ across all temperature conditions. This confirmed that the saponification had an overall reaction order of 2 and was therefore deemed a second-order kinetic reaction. The $C_{18}H_{34}O_2$:$CaCl_2$ mass ratio (Figure 6-a) was converted into concentration; the results revealed that at a pH value of 5, reaction temperature of 30°C and reaction duration of 60 min, the saponification extents of FOG deposits corresponding to $C_{18}H_{34}O_2$:$CaCl_2$ concentration ratios of 1:0.5, 1:2.5, 1:3.0 and 1:3.5 were 8.0%, 17.0%, 23.8% and 24.8%, respectively. This demonstrated a strong linear correlation between $Ca^{2+}$ concentration and the saponification extent of FOG deposits, yielding the inference that $n$ = 1. As saponification followed a second-order reaction, the inference of $n$ = 1 consequently indicated that $m$ = 1.

The second-order reaction kinetics between $C_{18}H_{34}O_2$ and $CaCl_2$ determined herein are consistent with those reported previously. This is because the reaction between FFAs and $Ca^{2+}$ that induced FOG deposit formation is essentially the same as typical saponification, wherein nucleophilic addition and elimination occur successively. However, the reaction orders of specific reactants show minor discrepancies as Table 10. For instance, Grunvald et al. [42] proposed that both soybean oil and NaOH exhibited first-order reaction kinetics during their interaction, with NaOH primarily providing alkaline conditions for the saponification of soybean oil. Zhang et al. [43] suggested that NaOH exerted negligible influence on the saponification of lutein ester, consequently assigning a reaction kinetics order of 0 to NaOH and 2 to lutein ester. Notably, these reactions occurred in liquid–liquid homogeneous systems. Meanwhile, Pečar & Goršek [44] reported that in a liquid–liquid heterogeneous system, the reaction rates were influenced by both chemical reaction and mass transfer, resulting in discrepancies compared with previous studies. Herein, both $C_{18}H_{34}O_2$ and $CaCl_2$ acted as reactants and their concentrations exhibited approximately linear correlations with the saponification extent, indicating their first-order reaction kinetics. This further confirmed the equivalent importance and contribution of FFAs and $Ca^{2+}$ during the formation of fatty acid calcium deposits.

**Table 10. Comparison results of reaction kinetics orders**

| Reference | Species 1 of reactant (corresponding reaction order) | Species 2 of reactant (corresponding reaction order) | Species of Product (total reaction order) |
|---|---|---|---|
| Grunvald et al. [42] | Soybean oil (first-order) | NaOH (first-order) | Soft soap (second-order) |
| Zhang et al. [43] | Lutein ester (second-order) | NaOH (zero-order) | Lutein (second-order) |
| Pečar & Goršek [44] | Ethyl benzoate (zero-order) | NaOH (second-order) | Sodium benzoate (second-order) |
| This study | Oleic acid (first-order) | $CaCl_2$ (first-order) | Fatty acid calcium (second-order) |

The $k$ values were calculated at different temperature based on $\frac{1}{C_{\mathrm{FFA}}}$-$t$, with the results shown in Figure 6-c. Then, linear regression analysis was conducted on the data presented in Figure 6-c. Outlier data points were excluded to ensure that $R^2 \geq 0.9$. Accordingly, the slope $k'$ was obtained. Based on the equation $k' = k(\frac{1}{2})^n$, the $k$ values at 0°C, 10°C, 15°C and 25°C was 0.0032, 0.0118, 0.0134 and 0.0236, respectively, with corresponding $R^2$ values of 0.95, 0.90, 0.90 and 0.98; indicating excellent fits. The $k$ value progressively increased with temperature within the 0°C–25°C range, reaching its maximum at 25°C. Strong linear correlations were observed under all four temperatures, aligning with second-order reaction kinetics. The relation between the reciprocal of thermodynamic temperature ($\frac{1}{T}$) and logarithm of curve slope ($ln\ k$) was further investigated, with the calculation results presented in Table 11. Figure 7 is plotted based on the calculation results.

**Table 11. $k$ values at four different thermodynamic temperatures**

| $T$ (K) | $\frac{1}{T}$ ($K^{-1}$) | $k$ | $ln\ k$ |
|---|---|---|---|
| 298.15 | 0.0034 | 0.0236 | -3.75 |
| 303.15 | 0.0033 | 0.0134 | -4.31 |
| 313.15 | 0.0032 | 0.0118 | -4.44 |
| 323.15 | 0.0031 | 0.0032 | -5.74 |

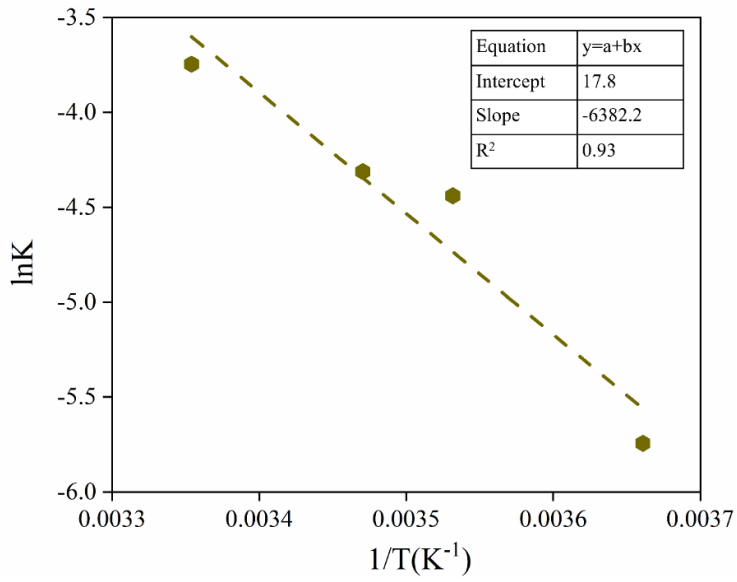


**Figure 7. $\frac{1}{T}$–$ln\ k$ at four different thermodynamic temperatures**

As shown in Figure 7, the slope $-\frac{E_a}{R}$ was measured as −6382.2. By substituting $R$ = 8.314 J·mol$^{-1}$·K$^{-1}$, $E_a$ was calculated as 53.1 kJ·mol$^{-1}$. The slope of the dashed curve was calculated then as $ln\ A$ = 17.8, from which $A$ was obtained as 5.4 × 10$^7$ L·mol$^{-1}$·min$^{-1}$ was obtained. By incorporating $m$ = 1, $n$ = 1, $E_a$ and $A$ into the Arrhenius equation, the kinetic equation for the reaction between FFAs and $Ca^{2+}$ was obtained as follows:

$$r = kC_{\mathrm{FFA}}C_{\mathrm{Ca^{2+}}} = 5.4 \times 10^7 \times e^{(-\frac{6382.2}{T})}C_{\mathrm{FFA}}C_{\mathrm{Ca^{2+}}} \quad (16)$$

## 4. Conclusions

This study systematically investigated the key factors and mechanisms governing the chemical formation of FOG deposits. By elucidating the intrinsic relations between these critical factors and FOG deposit formation, it provided scientific foundations for addressing pipe blockages in kitchen drainage systems. Saponification was determined as the key chemical process driving FOG deposit formation, and its extent was considerably influenced by multiple factors. Amongst the tested analytical methods, GC–MS demonstrated the highest accuracy in quantifying saponification and was therefore used for subsequent experiments. Single-factor experiments revealed that $C_{18}H_{34}O_2$ was the most dominant FFA species participating in saponification, with the optimal conditions for saponification as follows: $C_{18}H_{34}O_2$:$CaCl_2$ mass ratio of 1:1.40, pH value of 7, temperature of 30°C and reaction duration of 1440 min. Further, RSM revealed that the maximum saponification extent was only 77.932% at a reaction duration of 1035.283 min, $C_{18}H_{34}O_2$:$CaCl_2$ mass ratio of 1:1.481, pH value of 6.895 and reaction temperature of 25.170°C. These findings indicated that realistic kitchen drainage systems operating under these conditions may experience accelerated FOG deposit formation, causing increased pipe blockages.

The kinetic model established that the saponification reaction followed second-order kinetics, with an $E_a$ value of 53.1 kJ·mol$^{-1}$ and $A$ value of 5.4 × 10$^7$ L·mol$^{-1}$·min$^{-1}$. Although this kinetic framework provided a theoretical basis for predicting FOG deposit formation under various environmental conditions, several limitations should be acknowledged. First, we employed $C_{18}H_{34}O_2$ as the sole model FFA, whereas real kitchen wastewater contains a mixture of FFAs ($C_{12}$–$C_{20}$). Although $C_{18}H_{34}O_2$ exhibited the highest saponification extent amongst the tested FFAs and is the most abundant FFA in real FOG deposits, the presence of less reactive FFAs and short-chain FFAs in mixed systems may reduce the overall saponification extent. Therefore, our findings provide an upper-bound reference for saponification kinetics. Future studies should investigate saponification kinetics using FFA mixtures with defined compositions and real kitchen wastewater to quantify the deviation from the upper-bound reported here. Second, the optimal $C_{18}H_{34}O_2$:$CaCl_2$ mass ratio (1:1.40) was determined empirically, as no systematic study has yet investigated the optimal $Ca^{2+}$ ratio specifically for kitchen wastewater systems. Future gradient experiments around this ratio are needed to refine this value. Third, the proposed mechanistic explanations for the optimal pH (7) and temperature (30°C) are partly speculative as direct detection of reaction intermediates (e.g. $RCOO^-$ or free $Ca^{2+}$) was not performed.

In situ spectroscopic techniques, including ATR-FTIR spectroscopy for $RCOO^-$ or the use of ion-selective electrodes for free $Ca^{2+}$, are needed to directly validate these mechanisms. Fourth, our kinetic model was developed under controlled laboratory conditions using a batch system with fixed initial $Ca^{2+}$ dosage, which may not fully represent the continuous and dynamic conditions of real drainage systems. For example, continuous $Ca^{2+}$ has always been released from sewer concrete corrosion in practical engineering. Notably, long-term pipe-scale experiments under continuous flow conditions are recommended to verify the applicability of our kinetic model to real sewer systems. Finally, the temperature range in this study was limited to 0°C–50°C, and the optimal temperature may vary with different FFA compositions or calcium sources.

Nevertheless, this study advances the existing theoretical framework of FOG deposit formation from engineering simulation and chemical perspectives as well as offers practical insights for mitigating pipeline blockages and optimizing wastewater treatment systems. However, future studies should investigate the structural mechanics of FOG deposit adhesion on pipe walls and the fluid dynamics of wastewater scouring to enhance the engineering applicability of this framework and further improve urban sanitation management.

## 5. Declarations

### 5.1. Author Contributions

Conceptualization, Z.F. and X.Y.; methodology, J.F. and X.Y.; software, X.Y.; validation, X.Y. and Z.T.; formal analysis, Z.T. and X.Y.; investigation, J.F.; resources, Z.T.; data curation, X.Y.; writing—original draft preparation, X.Y.; writing—review and editing, D.R.; visualization, D.R.; supervision, Z.F.; project administration, Z.F.; funding acquisition, Z.F. All authors have read and agreed to the published version of the manuscript.

### 5.2. Data Availability Statement

The data presented in this study are available in the article.

### 5.3. Funding

This research has been supported by Henan Provincial Science and Technology Research Project (grant no. 252102321047), National Key R&D Program of China (grant no. 2024YFC3810901-05), National Key R&D Program of China (grant no. 2024YFC3810903-01), Key Promotion Project of Henan Province (No. 262102321051) and Henan Outstanding Foreign Scientist Studio Project (No. GZS2026013).

### 5.4. Conflicts of Interest

The authors declare no conflict of interest.

## 6. References

[1] Abdelaal, A., & Hassini, S. (2026). Dynamic resilience quantification of urban drainage networks. Journal of Hydrology, 668, 134995. doi:10.1016/j.jhydrol.2026.134995.

[2] Hernández-Montelongo, R., Gutiérrez-Pulido, H., García-Sandoval, J. P., & Alvarado-Mendoza, A. G. (2026). Fats, Oils, and Grease (FOG) Management in the Restaurant Sector of the Guadalajara Metropolitan Area, Mexico. Resources, 15(3), 35. doi:10.3390/resources15030035.

[3] Otsuka, T., Yamazaki, H., Ankyu, E., Ahamed, T., Anda, M., & Noguchi, R. (2020). Elucidation of the mechanism of blockage in sewer pipes by fatty acid deposition and suspended solid. Water (Switzerland), 12(8), 2291. doi:10.3390/w12082291.

[4] Koch, M., Hamscher, G., & Brühl, L. (2025). Towards a better understanding of saponification for the determination of mineral oil hydrocarbons (MOH) in edible oils and fats – Evaluation and optimization of current protocols. Analytica Chimica Acta, 1376, 344591. doi:10.1016/j.aca.2025.344591.

[5] Hu, Z., Yadav, S., Hassell, K., Gao, L., & Pramanik, B. K. (2025). Fat, oil and grease - induced sewer blockages: Mechanisms, modelling and monitoring strategies. Water Research, 286, 124215. doi:10.1016/j.watres.2025.124215.

[6] Shin, H., Han, S., & Hwang, H. (2015). Analysis of the characteristics of fat, oil, and grease (FOG) deposits in sewerage systems in the case of Korea. Desalination and Water Treatment, 54(4–5), 1318–1326. doi:10.1080/19443994.2014.910141.

[7] Del Mundo, D. M. N., & Sutheerawattananonda, M. (2017). Influence of fat and oil type on the yield, physico-chemical properties, and microstructure of fat, oil, and grease (FOG) deposits. Water Research, 124, 308–319. doi:10.1016/j.watres.2017.07.047.

[8] Wu, K., Xu, W., Lu, J., Wang, C., Liao, J., & He, X. (2022). Saponification with calcium enhanced methane yield in anaerobic digestion of fat, oil, and grease: The essential role of calcium. Renewable Energy, 195, 1103–1112. doi:10.1016/j.renene.2022.06.055.

[9] Sultana, N., Roddick, F., Jefferson, B., Gao, L., Bergmann, D., Papalois, J., Guo, M., Tzimourtas, K., & Pramanik, B. K. (2024). Effectiveness of grease interceptors in food service establishments for controlling fat, oil and grease deposition in the sewer system. Science of the Total Environment, 912, 169441. doi:10.1016/j.scitotenv.2023.169441.

[10] Yusuf, H. H., Roddick, F., Jegatheesan, V., Jefferson, B., Gao, L., & Pramanik, B. K. (2024). Uncovering the impact of metals on the formation and physicochemical properties of fat, oil and grease deposits in the sewer system. Chemosphere, 364, 143033. doi:10.1016/j.chemosphere.2024.143033.

[11] Jansson, M. B., & Wadsborn, R. (2007). Calculation of the influence of carbonate concentration on the formation of fatty acid calcium soaps in pulp washing. Nordic Pulp & Paper Research Journal, 22(1), 35–41. doi:10.3183/npprj-2007-22-01-p035-041.

[12] Husain, I. A. F., Alkhatib, M. F., Jami, M. S., Mirghani, M. E. S., Zainudin, Z. Bin, & Hoda, A. (2014). Problems, control, and treatment of fat, oil, and grease (FOG): A review. Journal of Oleo Science, 63(8), 747–752. doi:10.5650/jos.ess13182.

[13] Iasmin, M., Dean, L. O., & Ducoste, J. J. (2016). Quantifying fat, oil, and grease deposit formation kinetics. Water Research, 88, 786–795. doi:10.1016/j.watres.2015.11.009.

[14] Wang, Z., Li, C. X., Qian, R., Liu, R., Chen, W. L., & Xu, K. X. (2020). Research on Vegetable Oils Classification Based on Two-Dimensional Correlation Near-Infrared Spectroscopy. Guang Pu Xue Yu Guang Pu Fen Xi/Spectroscopy and Spectral Analysis, 40(10), 3230–3234. doi:10.3964/j.issn.1000-0593(2020)10-3230-05.

[15] Zhou, W., Zhang, Y., Qi, H., Wang, Q., Yao, B., & Li, D. (2019). Optical properties of crude oil with different temperatures. Optik, 196, 162946. doi:10.1016/j.ijleo.2019.162946.

[16] Iasmin, M., Dean, L. O., Lappi, S. E., & Ducoste, J. J. (2014). Factors that influence properties of FOG deposits and their formation in sewer collection systems. Water Research, 49, 92–102. doi:10.1016/j.watres.2013.11.012.

[17] Kusum, S. A., Pour-Ghaz, M., & Ducoste, J. J. (2020). Reducing fat, oil, and grease (FOG) deposits formation and adhesion on sewer collection system structures through the use of fly ash replaced cement-based materials. Water Research, 186, 116304. doi:10.1016/j.watres.2020.116304.

[18] Mohana, A. A., Roddick, F., Periasamy, S., Gao, L., & Pramanik, B. K. (2025). Sustainable lipid extraction: green solvents and hydrotalcite as alternatives to conventional methods for measuring fatty acids in fat, oil and grease. Green Chemistry, 27(16), 4222–4234. doi:10.1039/d5gc00515a.

[19] Mahesar, S. A., Sherazi, S. T. H., Khaskheli, A. R., Kandhro, A. A., & Uddin, S. (2014). Analytical approaches for the assessment of free fatty acids in oils and fats. Analytical Methods, 6(14), 4956–4963. doi:10.1039/c4ay00344f.

[20] Wang, H., Hao, Q., Yu, L., & Li, G. (2011). The optimization of preparation of calcium salts of fatty acids from palm oil. Journal of Yangzhou University (Agricultural and Life Science Edition), 32(4), 70–77. doi:10.16872/j.cnki.1671-4652.2011.04.015.

[21] Yan, X., Guan, Y., & Fang, Z. (2023). Physical and chemical characteristics of fat, oil and grease deposits in Chinese kitchen drainage systems. Waste Management and Research, 41(3), 635–643. doi:10.1177/0734242X221123973.

[22] Larkin, P. J. (2018). Instrumentation and Sampling Methods. Infrared and Raman Spectroscopy, 29–61, Elsevier, Amsterdam, Netherlands. doi:10.1016/b978-0-12-804162-8.00003-3.

[23] Larkin, P. J. (2018). Environmental Dependence of Vibrational Spectra. Infrared and Raman Spectroscopy, 63–73, , Elsevier, Amsterdam , Netherlands. doi:10.1016/b978-0-12-804162-8.00004-5.

[24] Abu-Aqil, G., Adawi, S., & Huleihel, M. (2025). Early and swift identification of fungal-infection using infrared spectroscopy. Spectrochimica Acta - Part A: Molecular and Biomolecular Spectroscopy, 325, 125101. doi:10.1016/j.saa.2024.125101.

[25] Khan, F. U.-H., & Landskron, K. (2026). Mechanistic Insights Into Supercapacitive Swing Adsorption via Acid–Base Titrations. Small. doi:10.1002/smll.73437.

[26] Hassan, M. A., M.AlMutairi, A., N.AlFadhli, S., AlOtaibi, S. S., Alhussin, M. S., & Al Saeed, S. (2026). NEW and accurate analytical method for measuring mono-ammonium phosphate content in dry chemical extinguishing powder (Part I). Results in Chemistry, 103039. doi:10.1016/j.rechem.2026.103039.

[27] Duan, Y., Feng, J., Zhu, Y., Li, H., Liu, X., Zhou, H., & Li, W. (2018). A systematic approach to measure the contents of mono- and di-sulfonates in petroleum sulfonates by the novel method of acid-base titration coupled with traditional two-phase titration. RSC Advances, 8(67), 38606–38613. doi:10.1039/c8ra05816d.

[28] Lolli, V., Dall'Asta, M., Caligiani, A., Del Rio, D., de la Fuente, M. A., & Gómez-Cortés, P. (2022). Detection of cyclopropane fatty acids in human breastmilk by GC-MS. Journal of Food Composition and Analysis, 107, 104379. doi:10.1016/j.jfca.2021.104379.

[29] Walczak, J., Bocian, S., Kowalkowski, T., Trziszka, T., & Buszewski, B. (2017). Determination of Omega Fatty Acid Profiles in Egg Yolk by HILIC-LC-MS and GC-MS. Food Analytical Methods, 10(5), 1264–1272. doi:10.1007/s12161-016-0655-7.

[30] Fang, J., Dong, X., Zhao, X., He, J., DE, S., Liang, C., Li, C., Ji, L., Zhang, L., Chen, Z., Liu, L., & Guo, W. (2026). Dynamics of flavor compounds in raw milk and infant formula: Delivery, formation, and evolution. LWT, 247, 119346. doi:10.1016/j.lwt.2026.119346.

[31] Vasiliki, G., Konstantina, F., Olga, B., Georgios, T., Helen, G., & Chistina, V. (2026). GC-MS method development and validation for the determination of Short Chain Fatty Acids in human feces. Journal of Pharmaceutical and Biomedical Analysis, 277, 117488. doi:10.1016/j.jpba.2026.117488.

[32] Chanakaewsomboon, I., Tongurai, C., Photaworn, S., Kungsanant, S., & Nikhom, R. (2020). Investigation of saponification mechanisms in biodiesel production: Microscopic visualization of the effects of FFA, water and the amount of alkaline catalyst. Journal of Environmental Chemical Engineering, 8(2), 103538. doi:10.1016/j.jece.2019.103538.

[33] Ulfa, M., & Eka Cahyani, D. (2019). Synthesis and Properties of Soaps from Bidara leaf (Ziziphus mauritania) Via Soft Saponification. Oriental Journal of Chemistry, 35(2), 892–896. doi:10.13005/ojc/350254.

[34] Gomes, L. C., Alcalde, C. R., Damasceno, J. C., Rigolon, L. P., Possamai, A. P. S., & Hygino, B. (2018). Concentrate containing calcium salts of fatty acids rich in polyunsaturated fatty acids can change rumen fermentation in grazing goats. Semina:Ciencias Agrarias, 39(6), 2621–2634. doi:10.5433/1679-0359.2018v39n6p2621.

[35] Kamiya, Y., Suzuki, T., Oikawa, K., Kobayashi, D., & Fujioka, K. (2025). Effects of Calcium Salts of Fatty Acids on Lactation, Rumen Fermentation, and Methane Emission in Dairy Cows. Animal Science Journal, 96(1), 70114. doi:10.1111/asj.70114.

[36] Rodrigues, H. P., Ferreira, J. M. de S., Pereira, M. I. B., Trajano, L. S., Souza, L. L., dos Santos Pina, D., de Freitas Junior, J. E., de Carvalho, G. G. P., Santos, S. A., & Azevêdo, J. A. G. (2026). Levels of starch and supplementation with calcium salts of palm oil fatty acids in the diets of goats and sheep. Small Ruminant Research, 254, 107661. doi:10.1016/j.smallrumres.2025.107661.

[37] Gurd, C., Villa, R., & Jefferson, B. (2020). Understanding why fat, oil and grease (FOG) bioremediation can be unsuccessful. Journal of Environmental Management, 267, 110647. doi:10.1016/j.jenvman.2020.110647.

[38] Sharif, K., & Gormley, M. (2021). Integrating the design of tall building, wastewater drainage systems into the public sewer network: A review of the current state of the art. Water (Switzerland), 13(22), 3242. doi:10.3390/w13223242.

[39] Xiao, H., Li, Y., & Wang, H. (2017). A stochastic kinetic study of preparing fatty acid from rapeseed oil via subcritical hydrolysis. Applied Energy, 204, 1084–1093. doi:10.1016/j.apenergy.2017.05.013.

[40] Uchida, H., & Kamijo, T. (2009). Measurement and correlation of the solid-liquid-gas equilibria for carbon dioxide + normal chain saturated aliphatic hydrocarbon systems. Journal of Supercritical Fluids, 51(2), 136–141. doi:10.1016/j.supflu.2009.08.007.

[41] Bertakis, E., Lemonis, I., Katsoufis, S., Voutsas, E., Dohrn, R., Magoulas, K., & Tassios, D. (2007). Measurement and thermodynamic modeling of solid–liquid–gas equilibrium of some organic compounds in the presence of CO2. The Journal of supercritical fluids, 41(2), 238-245. doi:10.1016/j.supflu.2006.10.003.

[42] Grunvald, A. K., De Carvalho, C. G. P., Leite, R. S., Mandarino, J. M. G., De Bastos Andrade, C. A., Amabile, R. F., & De Paulo Campos Godinho, V. (2013). Influence of temperature on the fatty acid composition of the oil from sunflower genotypes grown in tropical regions. JAOCS, Journal of the American Oil Chemists' Society, 90(4), 545–553. doi:10.1007/s11746-012-2188-6.

[43] Zhang, W. H., Wu, X. X., & Ma, K. J. (2013). Research progress of enhanced extracting natural products by ultrasonic technology. Xiandai Huagong/Modern Chemical Industry, 33(7), 26–29. doi:10.16606/j.cnki.issn0253-4320.2013.07.019.

[44] Pečar, D., & Goršek, A. (2015). Saponification reaction system: A detailed mass transfer coefficient determination. Acta Chimica Slovenica, 62(1), 237–241. doi:10.17344/acsi.2014.1110.